# Structure of the Bis($Mg^{2+}$)−ATP−Oxalate Complex of the Rabbit Muscle Pyruvate Kinase at 2.1 Å Resolution: ATP Binding over a Barrel[†,‡]

Todd M. Larsen, Matthew M. Benning, Ivan Rayment, and George H. Reed*

*Institute for Enzyme Research, Graduate School, and Department of Biochemistry, College of Agricultural and Life Sciences, University of Wisconsin−Madison, Madison, Wisconsin 53705*

*Received January 30, 1998; Revised Manuscript Received March 5, 1998*

ABSTRACT: Pyruvate kinase from rabbit muscle has been cocrystallized as a complex with $Mg^{II}$ATP, oxalate, $Mg^{2+}$, and either $K^+$ or $Na^+$. Crystals with either $Na^+$ or $K^+$ belong to the space group $P2_12_12_1$, and the asymmetric units contain two tetramers. The structures were solved by molecular replacement and refined to 2.1 ($K^+$) and 2.35 Å ($Na^+$) resolution. The structures of the $Na^+$ and $K^+$ complexes are virtually isomorphous. Each of the eight subunits within the asymmetric unit contains $Mg^{II}$oxalate as a bidentate complex linked to the protein through coordination of $Mg^{2+}$ to the carboxylates of Glu 271 and Asp 295. Six of the subunits also contain an $\alpha,\beta,\gamma$-tridentate complex of $Mg^{II}$ATP, and the active-site cleft, located between domains A and B, is closed in these subunits. In the remaining two subunits $Mg^{II}$ATP is missing, and the active-site cleft is open. Closure of the active-site cleft in the fully liganded subunits includes a rotation of 41° of the B domain relative to the A domain. α-Carbons of residues in the B domain undergo movements of up to 17.8 Å (Lys 124) in the cleft closure. Lys 206, Arg 119, and Asp 177 from the B domain move several angstroms from their positions in the open conformation to contact the $Mg^{II}$ATP complex in the active site. The γ-phosphate of ATP coordinates to both magnesium ions and to the monovalent cation, $K^+$ or $Na^+$. A $Mg^{2+}$-coordinated oxygen from the $Mg^{II}$oxalate complex lies 3.0 Å from Pγ of ATP, and this oxygen is positioned for an in-line attack on the phosphorus. The side chains of Lys 269 and Arg 119 are positioned to provide leaving-group activation in the forward and reverse directions. There is no obvious candidate for the acid/base catalyst near the 2-*si* face of the prospective enolate of the normal substrate. A functional group linked through solvent and side-chain hydroxyls may function in a proton relay.

The physiological reaction of pyruvate kinase, the final step in glycolysis, yields ATP and pyruvate from ADP, P-enolpyruvate,[1] and a proton. The initial step in the reaction is believed to be phosphoryl transfer from P-enolpyruvate to $Mg^{II}$ADP, producing bound $Mg^{II}$ATP and the enolate of pyruvate (*1*). The enolate is subsequently protonated on the 2-*si* face prior to release from the active site as the α-keto carboxylate product (*2*). Ketonization of enolpyruvate supplies the free energy that renders the reaction "metabolically" irreversible. The enzyme catalyzes enolization of pyruvate, the first step in the back reaction, in the presence of metal cofactors and ATP or $P_i$ or other "$P_i$-like" dianions (*3*). Despite the unfavorable equilibrium constant, the reverse reaction of pyruvate kinase can be demonstrated (*4*−*6*), although the $K_M$ for pyruvate is high (∼0.01 M).

The weak binding of pyruvate in the presence of ATP, dimerization of pyruvate at high concentrations (*7*), and an intrinsic, bicarbonate-dependent ATPase activity of the enzyme (*8*) hamper studies of enzymic complexes of ATP and pyruvate, which require extended incubation periods. In contrast, oxalate, an analogue of the enolate of pyruvate, binds to the enzyme with high affinity in the presence (*9*) or absence (*10*) of ATP. The robust complexes of pyruvate kinase, ATP, and oxalate have been exploited in spectroscopic studies, which have revealed information on the interaction of the enzyme and substrates with the 2 equiv of divalent cation which are obligatory cofactors in the reaction (*9*, *11*, *2*). Furthermore, synthetic oxalyl phosphate is a substrate for pyruvate kinase (*13*), and the ATP−oxalate complex represents the product of this reaction. The high affinity of oxalate for the enzyme also excludes bicarbonate from the active site and effectively eliminates the bicarbonate-dependent ATPase activity. Properties of the pyruvate kinase complex with ATP and oxalate make it an attractive candidate for high-resolution crystallographic studies.

Previous crystallographic studies of pyruvate kinase have revealed the four domain architecture of each of the four subunits that make up the functional tetramer (*14*, *15*). The N-terminal domain Ile12−Arg 42 consists of a short helix−turn−helix structure. The active site is located in a large cleft formed by the interface between two larger domains, the $\beta_8\alpha_8$ barrel or A domain and the β-barrel of the B domain.

[†] This research was supported in part by NIH Grants GM35752 (G.H.R.) and AR35186 (I.R.).

[‡] X-ray coordinates for these two complexes of pyruvate kinase have been deposited in the Brookhaven Protein Data Bank under file names 1A49 ($K^+$) and 1A5U ($Na^+$).

* Address correspondence to this author at the Institute for Enzyme Research, University of Wisconsin, 1710 University Ave., Madison, WI 53705.

[1] Abbreviations: P-enolpyruvate, phosphoenolpyruvate; ATPγS, adenosine 5′-*O*-(3-thiotriphosphate); ADPαS, adenosine 5′-*O*-(1-thiodiphosphate); EPR, electron paramagnetic resonance; NMR, nuclear magnetic resonance; Hepes, 4-(2-hydroxyethyl)-1-piperazineethanesulfonic acid; L-P-lactate, L-2-phospholactate.

S0006-2960(98)00243-8 CCC: $15.00 
Published on Web 04/16/1998

Table 1: Data Collection Statistics

| | $Na^+$ | $K^+$ |
|---|---|---|
| X-ray source[a] | SSRL 7−1 MAR | SSRL 7−1 MAR |
| no. of crystals used | 1 | 1 |
| maximum resolution ($d_{min}$, Å) | 2.35 | 2.1 |
| total reflections | 717 630 | 815 369 |
| independent reflections | 193 413 | 267 793 |
| theoretical no. of reflections | 216 128 | 301 829 |
| % completeness of data | 90 | 89 |
| % completeness of data in highest shell[b] | 74 | 78 |
| $R_{merge}$ (%) | 5.3 | 4.7 |
| $R_{merge}$ (%) in the highest resolution shell[b] | 16.4 | 21.2 |
| average $I/\sigma$ | 22.1 | 19.8 |
| unit cell parameters (Å) | | |
| *a* | 95.3 | 95.3 |
| *b* | 216.5 | 216.5 |
| *c* | 258.6 | 258.6 |

[a] Wavelength used for data collection was 1.080 Å. [b] The highest-resolution shell is as follows: 2.46−2.35 Å ($Na^+$−pyruvate kinase−$Mg^{II}$oxalate−$Mg^{II}$ATP) and 2.18−2.10 Å ($K^+$−pyruvate kinase−$Mg^{II}$oxalate−$Mg^{II}$ATP).

The subunit interface is located in the C-terminal domain, which is a mixture of α and $\beta$ structure. The A and B domains are connected by a strand that emerges from the A domain at Gly 115 and a second strand that rejoins the A domain at Ala 219. The potential for a ligand-induced closure of the active-site cleft was recognized from the structures of pyruvate kinase−ligand complexes (*15*, *16*).

The primary sequence of pyruvate kinase does not contain motifs that are characteristic of any of the presently known families of nucleotide binding proteins (*17*, *18*). None of the published high-resolution structures of pyruvate kinase has contained a metal−nucleotide complex. Hence, the mode of binding of ATP to pyruvate kinase is of special interest. The bis($Mg^{2+}$) complexes of pyruvate kinase with ATP, oxalate, and either $Na^+$ or $K^+$ have been cocrystallized. The crystals diffract to high resolution. The present paper reports the molecular structures of these complexes.

## EXPERIMENTAL PROCEDURES

*Crystallization and Data Collection.* Rabbit muscle pyruvate kinase was isolated following the protocol of Teitz and Ochoa (*8*). Solutions of the protein were chromatographed over an S-300 gel-filtration column equilibrated with 10 mM Hepes-KOH, pH 7.0, and 0.1 M NaCl or KCl depending on the complex to be studied. Single crystals of pyruvate kinase complexed with $Na^+$, oxalate, $Mg^{2+}$, and ATP were grown at room temperature by the batch method from 7.1 mg/mL protein, 7.8% PEG 8000, 0.16 M NaCl, 5 mM $MgCl_2$, 5 mM ATP, 1 mM oxalate, and 50 mM succinate, pH 6.0. Rodlike crystals ~ 0.1 × 0.3 × 0.6 mm grew within 3 days. The crystals belong to the space group $P2_12_12_1$. The unit cell dimensions are $a = 95.3$ Å, $b = 216.5$ Å, and $c = 258.6$ Å. The asymmetric unit contains two tetramers.

The protocol for growing crystals of the pyruvate kinase complex with $K^+$, oxalate, $Mg^{2+}$, and ATP employed the same conditions as described for the complex of $Na^+$, except that KCl replaced NaCl. Crystals of the corresponding complex with $K^+$, however, did not grow spontaneously. To obtain these crystals, the crystallization mixture was micro-

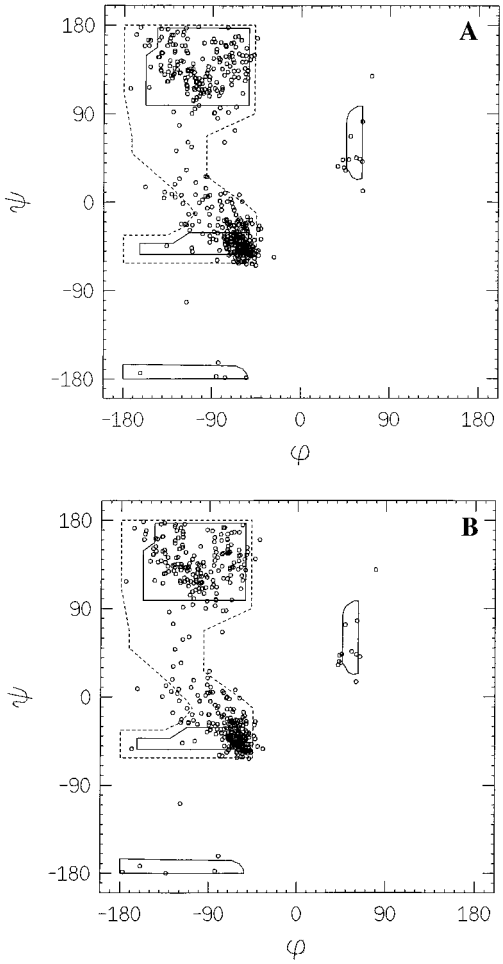


FIGURE 1: Ramachandran plots of the main-chain nonglycinyl dihedral angles of subunit 1 for the $Na^+$−pyruvate kinase−$Mg^{II}$-oxalate−$Mg^{II}$ATP complex (A) and the $K^+$−pyruvate kinase−$Mg^{II}$-oxalate−$Mg^{II}$ATP complex (B). Fully allowed $\phi$ and $\psi$ values are shown by solid enclosures. Partially allowed regions are enclosed by broken lines. For both complexes the most severe left-handed outlier is Thr 327 and the most severe right-handed outlier is Ser 361. Analysis of the Ramachandran plot of the $K^+$ complex with the program PROCHECK (*45*) showed that 90.2% of the residues were in fully allowed regions and 9.4% were in additional allowed regions. The same analysis of the $Na^+$ complex revealed that 90.0% of the residues were in fully allowed regions and 9.6% were in additional allowed regions.

seeded from crystals of the $Na^+$ complex 2 days after setup. Rodlike crystals grew within 3 days, and the crystals have the same morphology, space group, and cell dimensions as the seed crystals.

The transfer, freezing procedure, and data collection described below were applied to crystals of the complexes with either $Na^+$ or $K^+$. The crystals were transferred from the crystallization medium into a synthetic mother liquor containing 20% PEG 8000, 0.3 M salt (NaCl or KCl), 5 mM $Mg^{2+}$, 2mM oxalate, and 5 mM ATP in 50 mM succinate, pH 6.0 (solution A), for transport. Prior to freezing, each crystal was equilibrated with the cryoprotectant ethylene glycol. The equilibration was carried out by serial transfers of each crystal to solution A containing increasing concentrations of ethylene glycol. Initially, each crystal was moved to solution A that contained 10% ethylene glycol and allowed to equilibrate for 2 min. The crystal was transferred two additional times, first to solution A with 15% ethylene glycol

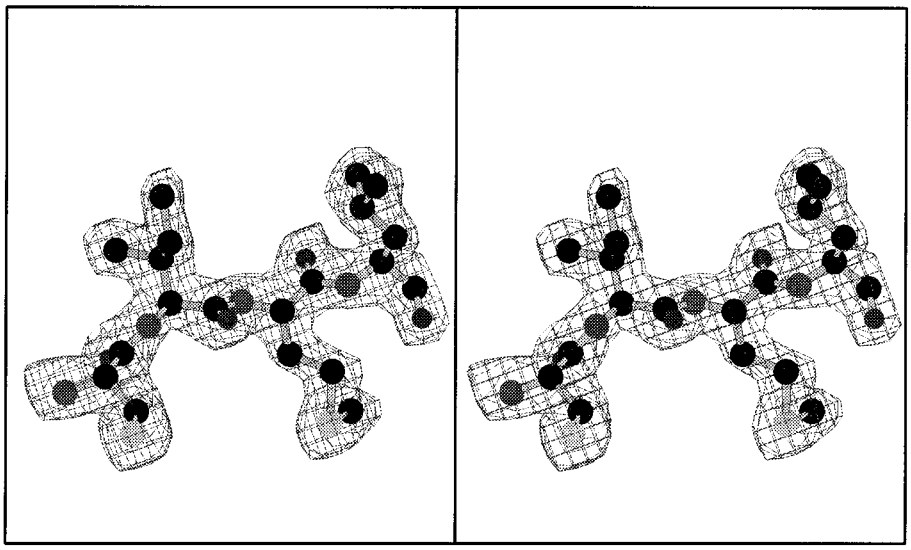

FIGURE 2: Representative portion from $2F_o - F_c$ electron density map of the $K^+$− pyruvate kinase−$Mg^{II}$oxalate−$Mg^{II}$ATP complex calculated with the final refined phases. Electron density for residues $^{357}$CIML of subunit 1 was contoured at 1$\sigma$. The program MOLDED (A. Fisher, unpublished results) was used to prepare this figure.

for 2 min and then to solution A with 20% ethylene glycol. The crystal was picked up within 20 s after addition to the 20% ethylene glycol solution in a loop of surgical suture and flash-frozen in a stream of $N_2$ at −160 °C (*19*, *20*). X-ray data were collected with a MAR detector from one frozen crystal of each complex on beamline 7-1 at Stanford Synchrotron Radiation Laboratory. Data collection statistics are summarized in Table 1.

*Molecular Replacement.* The three-dimensional structure of $Na^+$−pyruvate kinase−$Mg^{II}$oxalate−$Mg^{II}$ATP was solved by molecular replacement using the software package AMORE (*21*, *22*). X-ray coordinates of a tetramer of pyruvate kinase−$Mg^{2+}$−L-phospholactate (*16*) served as the search model. The rotation function revealed a symmetry-unique peak at a level of 8.7$\sigma$. A second symmetry-unique peak was present at a level of 7.6$\sigma$. The next largest peak in the map appeared at a level of 3$\sigma$. The translation function was applied to the two solutions. Rigid-body refinement was executed to refine the rotation and translation solutions, and the overall *R*-factor dropped from 50.7% to 41.4%. The final Eulerian angles and translation solutions were $\alpha = 167.1°$, $\beta = 18.86°$, $\gamma = 256.8°$, $a = 0.44$, $b = 0.15$, and $c = 0.09$ for solution I and $\alpha = 46.84°$, $\beta = 114.4°$, $\gamma = 107.2°$, $a = 0.48$, $b = 0.40$, and $c = 0.40$ for solution II.

*Refinement.* The structure of $Na^+$−pyruvate kinase−$Mg^{II}$-oxalate−$Mg^{II}$ATP was refined to 2.35 Å with the least-squares refinement program TNT (*23*), resulting in a drop in the crystallographic *R*-factor from 41.4% to 34.6%. Initial examination of the map using the molecular modeling program FRODO (*24*) revealed that all eight B domains were in conformations differing from those of the search model. Hence, all B domains were removed from the model, and a round of refinement was performed. The resulting $F_o - F_c$ density for the B domains of all subunits was well defined to 3$\sigma$. The $F_o - F_c$ density was used to build in the residues of the B domains using FRODO. Another cycle of refinement, following addition of all eight B domains reduced the *R*-factor to 27.9%. Further manual adjustments in the model were made with FRODO and O (*25*). Regions of density corresponding to $Mg^{II}$oxalate and to $Na^+$ were clearly present in all eight subunits. Density corresponding to $Mg^{II}$ATP was clearly present in subunits 1 and 3−7. Oxalate, ATP, and the metal ions were included in the model at this point. Water molecules were added to the model after another round of least-squares refinement and manual adjustment. The positions of the ordered water molecules were determined using the peak search algorithm in the TNT package. Following completion of manual adjustments and inclusion of waters, the model was refined, excluding the metal ions, oxalate, and ATP. The resulting $F_o - F_c$ electron density confirmed the positions of the metal ions, oxalate, and ATP, which were returned to the model for a final round of refinement. The current *R*-factor including all data to 2.35 Å resolution is 19.0%. The present model with two tetramers includes 1810 water molecules (temperature factor < 85). The rms deviations from "ideal" geometry are 0.013 Å for bond lengths, 2.1° for bond angles, and 0.007 Å for coplanar groups.

Initial phases for the complex of $K^+$−pyruvate kinase−$Mg^{II}$oxalate−$Mg^{II}$ATP were calculated from the refined coordinates of the $Na^+$−pyruvate kinase−$Mg^{II}$oxalate−$Mg^{II}$-ATP structure, leaving out the metal ions, ATP, oxalate, and water molecules. Crystallographic least-squares refinement using the program TNT reduced the *R*-factor to 29.4% for all data to 2.1 Å. Manual adjustments in the model were made with the program O. Metal ions, ATP, and oxalate were then included in the model. Water molecules were added to the model after a cycle of refinement and manual adjustments. Strategies for further refinement of the model were the same as described for the corresponding model of the complex with $Na^+$. The current *R*-factor including all data to 2.1 Å resolution is 19.8%. The present model with two tetramers includes 1923 water molecules (temperature factor < 85). The rms deviations from "ideal" geometry are 0.022 Å for bond lengths, 2.0° for bond angles, and 0.012 Å for coplanar groups. Ramachandran plots for subunit 1 main-chain nonglycinyl dihedral angles of the complexes of $Na^+$ and $K^+$ are shown in Figure 1, panels A and B, respectively.

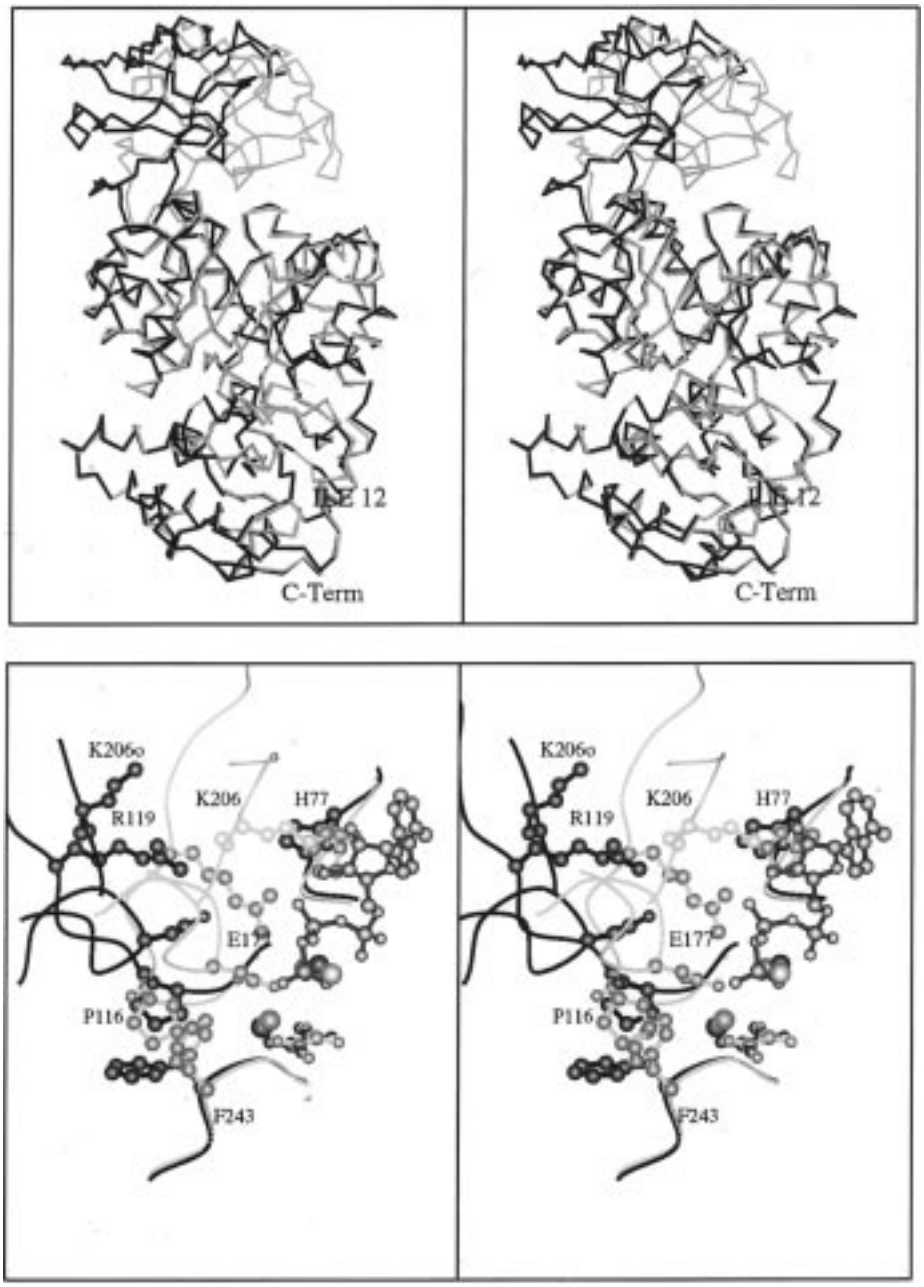


FIGURE 3: (a, top) Overlay of the α-carbons of subunits 5 and 8. Subunit 5, shown in gold, has a closed active-site cleft. Subunit 8, shown in green, has an open active-site cleft. (b, bottom) Overlay of the active site of subunits 5 and 8. Subunit 5 is shown in gold and subunit 8 is shown in green. A ball-and-stick model of $Mg^{II}ATP$ present in subunit 5 is shown in red/metallic brown. The green and gold spheres behind the $\gamma$-phosphate of ATP represent $K^+$ in the open and closed clefts, respectively. Lys 206 in the open conformation (green) is labeled K206o. The program MOLSCRIPT (*46*) was used to prepare this figure.

## RESULTS AND DISCUSSION

Only subtle differences were observed in the structures of the complexes with $K^+$ and $Na^+$. Figure 2 illustrates representative electron density calculated from the coefficients $2F_o - F_c$ for the complex with $K^+$. All residues in each of the eight subunits of both complexes (with the exception of some surface residues and residues 1−11) have well-defined side chains. The overall chain topology of each subunit is identical to that described previously (*15*).

A distinguishing characteristic of the structure is the variety of subunit conformations within the asymmetric unit. Changes in the positions of the B domains (residues 116−218), relative to the remainder of the protein, account for the various conformations. Movement of the B domain can be described as a pure rotation of the α-carbons about a unique axis. The angle of rotation determines the volume of the active-site cleft in the interface between the A and B domains. The active-site cleft is closed in subunits 1, 3−5, and 7. The cleft of subunit 6 is slightly opened, with the B domain having an angle of rotation of 11° relative to the closed subunits. The clefts of subunits 2 and 8 are open, and in these subunits the B domain exhibits an angle of rotation of 41° relative to the closed subunits (Figure 3a). The subunits that have the closed conformation (1 and 3−7) all have $Mg^{II}ATP$ bound in their active sites; whereas the subunits that have the open conformation (2 and 8) do not have $Mg^{II}ATP$ in their active sites. Pro 116, located in the region linking subunits A and B, is an indicator for the cleft

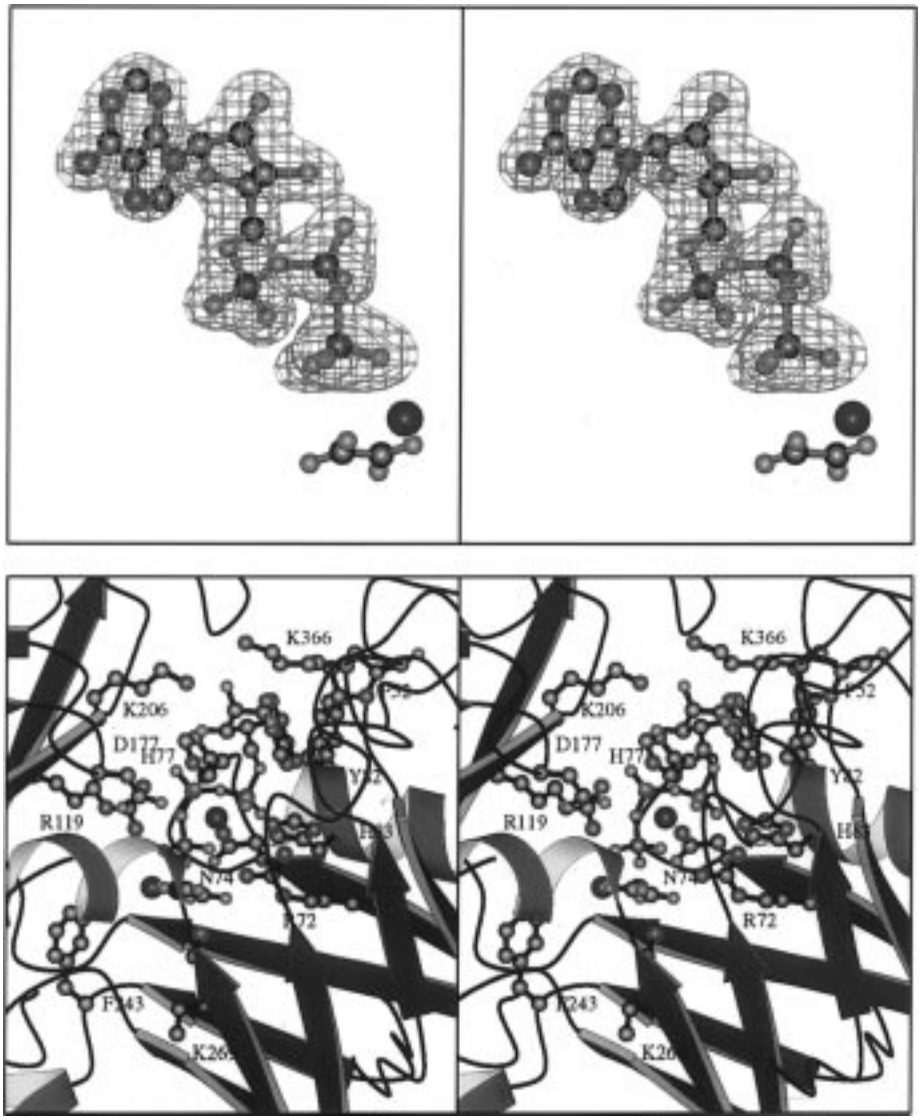


FIGURE 4: (a, top) $F_o - F_c$ electron density map contoured at $4\sigma$ for ATP of the $K^+$−pyruvate kinase−$Mg^{II}$oxalate−$Mg^{II}$ATP complex (subunit 5). A ball-and-stick model of ATP is shown in the density. The $Mg^{II}$oxalate complex is also shown as a ball-and-stick model. The program MOLDED (A. Fisher, unpublished results) was used to prepare this panel. (b, bottom) Ribbon representation of the closed active site of the $K^+$−pyruvate kinase−$Mg^{II}$oxalate−$Mg^{II}$ATP complex (subunit 5). Significant residues are represented by ball-and-stick models. For simplicity, water molecules were not included. Color codes: green, $Mg^{2+}$; violet, $K^+$; purple, phosphorus; red, oxygen; blue, nitrogen; gray, carbon. The program MOLSCRIPT (*46*) was used to prepare this panel.

closure. The $\phi$, $\psi$ values for Pro 116 range from −62°, 58° to −67°, 68° for the closed conformations and from −59°, 142° to −65°, 152° for the open conformations (see Table 2). The orientation of the phenyl ring of Phe 243 from the A domain flips up toward the active site in the closed clefts (Figure 3b). The flip of the Phe ring avoids a close contact with Pro 116 in the closed conformation.

*Active Site of the Closed Subunits.* Difference electron density ($F_o - F_c$) of ATP from the active site of subunit 5 of the complex with $K^+$ is shown in Figure 4a. The difference density of Figure 4a was generated by excluding ATP from the refinement and phase calculation. The density exhibits well-defined lobes for the phosphate and ribose oxygens and for the exocyclic amino nitrogen of adenine. A ball-and-stick model of ATP is shown in the density. Figure 4b shows the active site of the closed subunit for the $K^+$ complex.

*Metal Ion Coordination in the Closed Subunits.* Coordination of the inorganic cations in the subunits with ATP is summarized in Figure 5a. The $Mg^{II}$oxalate complex is bound to the protein through coordination of $Mg^{2+}$ to the carboxyl-

Table 2: Unit Cell Contents and Domain Orientations within Subunits

| subunit | $\phi$, $\psi$ values of Pro 116 (deg) | active site contains $Mg^{II}$ATP | rotation angle, $\theta$, of the B domain relative to the A domain[a] (deg) |
|---|---|---|---|
| 1 | −67, 68 | + | 0 |
| 2 | −59, 152 | − | 41 |
| 3 | −62, 66 | + | 1 |
| 4 | −68, 68 | + | 1 |
| 5 | −68, 59 | + | 0 |
| 6 | −65, 68 | + | 11 |
| 7 | −65, 58 | + | 1 |
| 8 | −65, 142 | − | 41 |
| 1 (L-P-lac)[b] | −61, 60 | | 21 |
| 8 (L-P-lac)[b] | −65, 150 | | 45 |

[a] Referenced to subunit 1, where $\theta = 0°$. [b] Angles correspond to $\phi$,$\psi$ values of Pro 116 and domain rotations in subunits 1 and 8 of the complex of pyruvate kinase, L-P-lactate, $Mg^{2+}$, and $K^+$ (*16*).

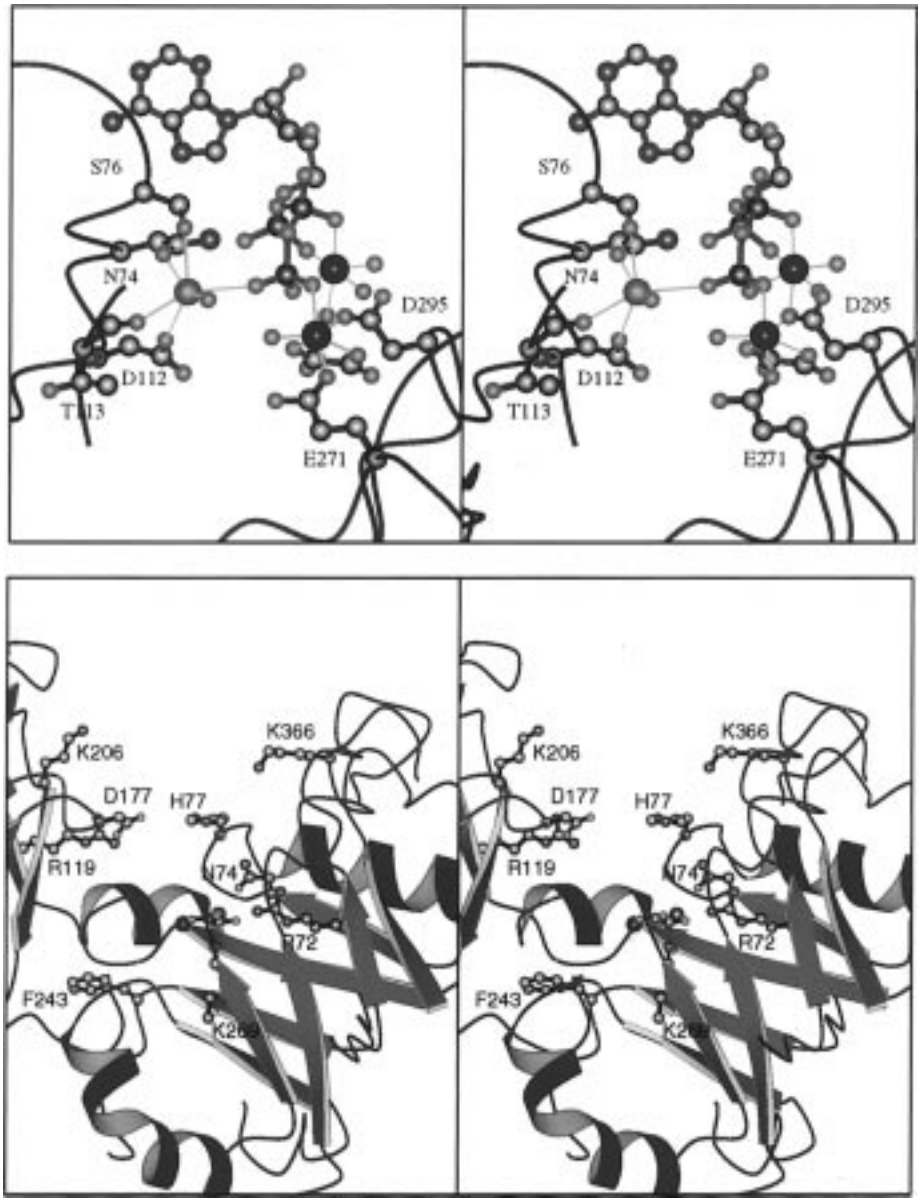


FIGURE 5: (a, top) Ball-and-stick model of the $K^+$−pyruvate kinase−$Mg^{II}$oxalate−$Mg^{II}$ATP complex closed active site (subunit 5). The coordination of the inorganic cations is shown by the orange lines. The $Mg^{2+}$ to ligand distances range from 2 to 2.3 Å and the $K^+$ to ligand distances range from 2.6 to 3.0 Å. (b, bottom) Ribbon representation of the $K^+$−pyruvate kinase−$Mg^{II}$oxalate−$Mg^{II}$ATP complex open active site (subunit 8). Ball-and-stick models represent important residues. For simplicity, water molecules are not included. The program MOLSCRIPT (*46*) was used to prepare this figure.

ate side chains of Glu 271 and Asp 295. The carboxylate ligands to the metal ion, $Mg^{2+}$ or $Mn^{2+}$, are present in the structures of complexes of the enzyme with L-phospholactate and pyruvate, respectively (*15*, *16*). The $Mg^{II}$oxalate complex is bidentate, and the other ligands in the octahedral coordination sphere of $Mg^{2+}$ are an oxygen from the $\gamma$-phosphate of ATP and a water molecule. The coordination scheme of $Mg^{2+}$ at this site is identical to that determined by EPR spectroscopy for $Mn^{2+}$ in metal hybrid complexes of pyruvate kinase with $Mg^{II}$ATP and oxalate (*9*).

The triphosphate chain of ATP is "curled" due to its $\alpha,\beta,\gamma$-tridentate coordination to $Mg^{2+}$. The stereochemical configuration of the $Mg^{II}$ATP complex is consistent with the results from studies with isomers of exchange-inert $Rh^{III}$-ATP complexes (*26*) and with the stereoselectivity observed for nucleoside phosphorothioate substrates (*27*). The octahedral coordination sphere of this second $Mg^{2+}$ is completed by three water molecules. The stereochemistry of the bis-($Mg^{2+}$) coordination to the $\gamma$-phosphate is identical to that observed in complexes of $Mn^{2+}$ and $Mg^{2+}$ with epimers of [$\gamma$-$^{17}$O]ATP$\gamma$S (*12*). As found in two other complexes of pyruvate kinase (*15*, *16*), the monovalent cation, $K^+$ or $Na^+$, coordinates to four protein ligands: the carbonyl of Thr 113; the hydroxyl of Ser 76, the carboxylate of Asp 112, and the carboxamide oxygen of Asn 74. The monovalent cation also coordinates to an oxygen from the $\gamma$-phosphate of ATP. A sixth ligand to the monovalent cation, a water molecule, is discernible in all of the subunits that contain ATP except for subunit 1 in the complex of $K^+$ and subunit 3 in the complex of $Na^+$.

In the subunits containing ATP, each of the three peripheral oxygens of the $\gamma$-phosphate moiety coordinates to one of the three inorganic cations in the active site. The $\gamma$-phosphate bridge between the two divalent cations was detected earlier in EPR studies of the ATP/oxalate complex (*9*). The possibility that the monovalent cation coordinated

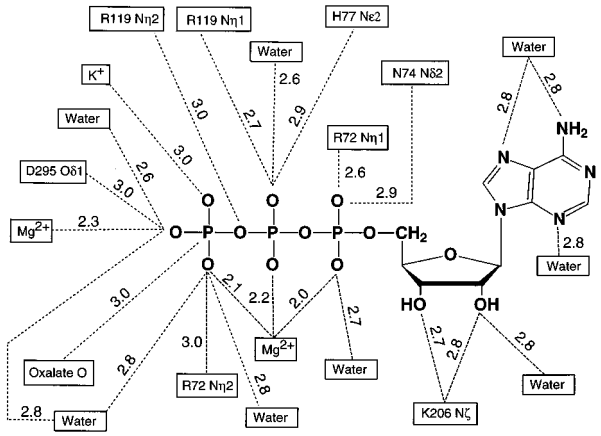


FIGURE 6: Schematic drawing showing metal ion coordination and other interactions of ATP in the $K^+$−pyruvate kinase−$Mg^{II}$oxalate−$Mg^{II}$ATP complex (subunit 5). Interatomic distances are given in angstroms. The oxalate oxygen labeled as oxalate O is the "nucleophilic" oxygen.

to the third oxygen was suggested on the basis of EPR studies of $Mn^{2+}$ complexes with the epimers of [$\gamma$-$^{17}$O]ATP$\gamma$S (*12*). The average distances between cations for the complex in the closed subunits are 5.0−5.1 Å between magnesium ions; 5.4 Å between $Mg^{2+}$ coordinated to oxalate and $K^+$ or $Na^+$; and 6.9−7.0 Å between $Mg^{2+}$ coordinated to ATP and $K^+$ or $Na^+$.

*Binding of $Mg^{II}$ATP.* When the B domain rotates to close the active-site cleft, the side chains of three residues from the B domain move several angstroms from their positions in the open conformation to make contact with $Mg^{II}$ATP (Figure 3b). Nζ of Lys 206 moves 10.4 Å to a position between the 2′- and 3′-hydroxyls of the ribose moiety; the guanidinium moiety of Arg119 moves 6.8 Å to lie within H-bonding distance of the $\beta$-phosphate of the ATP; and the carboxylate of Asp 177 travels 6.8 Å to H-bonding contact with a water of hydration on the $Mg^{2+}$ of $Mg^{II}$ATP. As indicated in Figure 4b, the substrates and metal ions are located at the C-terminal end of the $\beta_8\alpha_8$ barrel. The adenine ring fits into a pocket bounded on one side by His 77 and the edge of Pro 52 on the other. Tyr 82 lies at the end of the pocket but is not stacked with the adenine ring. The exocyclic amino group of adenine does not have a clear H-bonding partner, and the absence of a definite H-bonding interaction for this group is consistent with the rather broad nucleotide specificity of the enzyme (*28*). Potential H-bonding interactions of ATP with protein ligands are the N$\eta$1 and N$\eta$2 of Arg 72, N$\delta$2 of Asn 74, N$\eta$1 and N$\eta$2 of Arg 119, and Nζ of Lys 206. The side chain of Lys 366 lies above the ribose ring. The proximity of Lys 366 to the ribose of the nucleotide substrate was detected in earlier active-site-directed, chemical modification experiments with the ADP dialdehyde affinity reagent (*29*). A summary of groups making close contact with ATP is provided in Figure 6.

As expected from its primary sequence, the ATP complex of pyruvate kinase does not fit the patterns of binding interactions that are characteristic of the superfamilies of nucleotide binding proteins (*17*, *18*) or of an "ATP-binding structural motif" (*30*). Moreover, the ATP−oxalate complex of pyruvate kinase does not have a great deal in common with the ATP−oxalate or the ATP−pyruvate complex of P-enolpyruvate carboxykinase from *E. coli* (*31*, *32*).

*Active Site of the Open Subunits.* Density corresponding to $Mg^{II}$ATP is not present in the subunits that have an open cleft. In these two subunits the active site contains $Mg^{II}$-oxalate and the monovalent cation. Figure 5b shows the active site of the open subunit of the $K^+$ complex. As found for the subunits with ATP bound, in the subunits with the open clefts, $Mg^{2+}$ of the oxalate complex coordinates to the carboxylate side chains of Glu 271 and Asp 295 and two water molecules. The coordination sphere of the monovalent cation in the subunits with open clefts is the same as in those with closed clefts, except that a water molecule replaces the oxygen of the $\gamma$-phosphate of ATP to complete the coordination shell. The separation between the monovalent cation and the $Mg^{2+}$ coordinated to oxalate is slightly larger than in the closed subunits, 5.8 Å for $K^+$ and 5.6 Å for $Na^+$.

The $k_{cat}$ of $Na^+$ activation of pyruvate kinase is about 8% that of $K^+$ (*33*). Within the resolution limits of the two structures, however, the complexes with $Na^+$ and with $K^+$ are virtually indistinguishable−backbone and side-chain atoms superimpose. The rms deviation of α-carbons in the superimposed structures is 0.08 Å.

The presence of only three $Mg^{II}$ATP molecules per tetramer in the crystal lattice was a somewhat surprising observation. Although crystal lattice forces might be responsible for the absence of "saturation" of active sites with the $Mg^{II}$ATP complex, there may be some aspect of negative cooperativity in binding of the nucleotide in play. The presence of completely and incompletely liganded subunits within the same asymmetric unit, however, permits a clear view of the changes in the structure that occur when $Mg^{II}$-ATP binds in the active site.

*Mechanistic Suggestions.* As noted above, the ATP−oxalate complex of pyruvate kinase represents the products complex of the reaction of the alternative substrate, oxalyl phosphate and ADP (*13*). One of the oxygen atoms from oxalate (O2) is positioned 3 Å from $P_\gamma$ of ATP (see Figure 7). This oxygen is in position for a direct in-line transfer of the phosphoryl group from ATP to oxalate, and a direct transfer is compatible with the known stereochemical course of the reaction (*34*).

Coordination of each peripheral oxygen of the $\gamma$-phosphate to one of the three inorganic cofactors is a distinctive feature of this complex. The three metal ions are in proper position to screen Coulombic repulsion between anionic reactants. Coordinate interactions of the peripheral oxygens with the positive charges of the inorganic cations could also be perceived to prepare the central phosphorus for a nucleophilic attack (*35*).

Two other interactions in the complex appear to be especially significant. The proximity of the guanidinium moiety of Arg 119 to the $\beta-\gamma$ bridging oxygen of ATP (3 Å) is suggestive of leaving-group activation by the positive charge of the Arg side chain in the direction of phosphoryl transfer from ATP. Furthermore, a $Mg^{2+}$ coordinates to the oxygen (O2, Figure 7) of oxalate that is the potential nucleophile in the ATP−oxalate to ADP−oxalyl phosphate direction. This $Mg^{2+}$ coordination, if preserved in the ADP−oxalyl phosphate (or P-enolpyruvate) complex, would provide leaving group activation in the other direction. Coordination between $Mg^{2+}$ and the oxygen in the C−O−P bridge is indicated in the complex of pyruvate kinase with the analogue of P-enolpyruvate, L-P-lactate (*16*). EPR spectro-

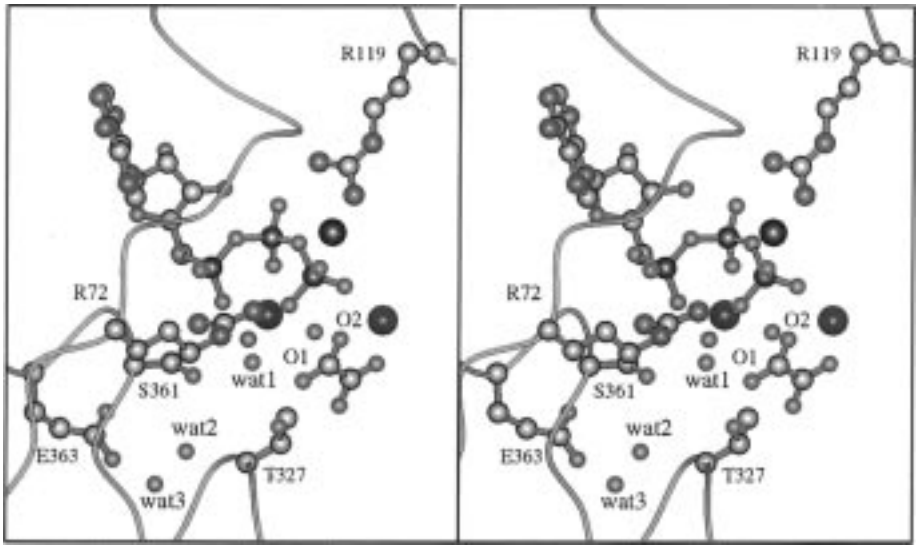


FIGURE 7: Stereoview of the $K^+$−pyruvate kinase−$Mg^{II}$oxalate−$Mg^{II}$ATP complex closed active site (subunit 5). Ball-and-stick models of residues having potential mechanistic roles are shown. Green spheres represent $Mg^{2+}$, and the dark blue sphere represents $K^+$. The program MOLSCRIPT (*46*) was used to prepare this figure.

scopic observations on $Mn^{2+}$ complexes of pyruvate kinase with P-enolpyruvate are compatible with a strained, four-member chelate ring interaction between $Mn^{2+}$ and the substrate (*36*). The $\epsilon$-amino group of Lys 269 is also close to the "nucleophilic" oxygen of oxalate and could participate in leaving-group activation as well as promote enolization of a bound pyruvate. Hence, there is potential for leaving-group activation in both directions of the reaction.

The identity of the group or groups responsible for general acid/base catalysis in the reaction remains somewhat elusive. The $\epsilon$-amino group of Lys 269 has previously been mentioned as a candidate for the acid/base catalyst (*6*, *14*). The side chain of Lys 269, however lies on the 2-*re* face of the prospective enolate (*15*, *16*) and this position is incompatible with the known stereochemistry of protonation (*2*). The proximity of the $\epsilon$-amino of Lys 269 to the "nucleophilic" oxygen of oxalate (O2, Figure 7) indicates that this group may participate in stabilizing the enolate and in leaving-group activation.

A water molecule that is in the coordination sphere of $Mg^{2+}$ of the $Mg^{II}$ATP (wat1, Figure 7) occupies the strategic position above the prospective 2-*si* face of the enolate of pyruvate (O1, Figure 7). Previous studies of the exchange of the methyl protons of pyruvate with solvent promoted by pyruvate kinase and metal ATP complexes indicated an electrophilic role of the divalent metal ions (*37*). Coordination of a divalent cation to pyruvate (*15*) is expected to promote enolization. Subsequent experiments with $Cr^{III}$ATP as the activator of exchange, however, also implicated the nucleotide-bound metal ion in activation of the acid/base catalyst (*38*). Enthusiasm for assignment of the $Mg^{2+}$-bound water as the catalyst is, however, restrained by the observation that $Co^{III}(NH_3)_4$ATP also promotes the exchange reaction at a rate only 3-fold lower than that of $Mg^{II}$ATP (*39*). Although the amine ligand in the $Co^{III}(NH_3)_4$ATP that would occupy the position analogous to that of the "catalytic water" ligand is in a trans position and exchanges with solvent rapidly above pH 5 (*40*), it is unlikely that a $Co^{III}$-$NH_2^-$ species participates in the enzyme-catalyzed exchange reaction owing to the low acidity of the amine ligand (*41*). It is possible that an alternative pathway for proton transfer becomes viable in the $Co^{III}(NH_3)_4$ATP complex. For example, in the exchange reaction of pyruvate promoted by phosphate and "phosphate-like anions" (*3*), the reaction rate correlates with the p$K_a$ of the anion. The nucleotide-bound metal and its waters of hydration are presumably missing in the phosphate-activated exchange.

More recent $^3$H-trapping experiments (*42*, *43*) and measurements of solvent $^2$H isotope effects (*43*) suggested the possibilty of a proton relay in the acid/base chemistry of pyruvate kinase. A proton relay might explain the absence of a clear candidate for the general acid/base catalyst proximate to the 2-*si* face of the prospective enolate. The side chains of the highly conserved residues, Ser 361, Thr 327, and Arg 72, project into the region above the 2-*si* face of the prospective enolate. The functional groups of these side chains could participate in a proton relay leading to a general acid/base catalyst somewhat removed from the site of proton addition and removal. Two water molecules (wat2 and wat3, Figure 7) "connect" the hydroxyls of Ser 361 and Thr 327 to the carboxyl(ate) of Glu 363, another highly conserved residue (Figure 7). The "buried" side chain of Glu 363 does not lie close to a source of positive charge and might function as the acid/base catalyst through a relay of bound water and the hydroxyls of Ser 361 or Thr 327. The water molecules and hydroxyl side chains could conserve a pool of $^3$H in the presence of a bound metal P-enolpyruvate complex and thus allow $^3$H trapping in the chase phase of the experiments (*43*). Alternatively, the guanidinium moiety of Arg 72 might constitute a small reservoir of relatively slowly exchanging $^3$H (*44*) that eventually gets trapped in pyruvate in the chase phase of the trapping experiments. Experiments with site-specific mutant forms of pyruvate kinase should assist in resolving these issues.

## REFERENCES

1. Seeholzer, S. H., Jaworowski, A., and Rose, I. A. (1991) *Biochemistry 30*, 727−732.

2. Rose, I. A. (1970) *J. Biol. Chem. 245*, 6052−6056.
3. Rose, I. A. (1960) *J. Biol. Chem. 235*, 1170−1177.
4. McQuate, J. T., and Utter, M. F. (1959) *J. Biol. Chem. 234*, 2151−2157.
5. Giles, I. G., Poat, P. C., and Munday, K. A. (1975) *Biochem. Soc. Trans. 3*, 312−314.
6. Dougherty, T. M., and Cleland, W. W. (1985) *Biochemistry 24*, 5875−5880.
7. Gallo, A. A., and Sable, H. Z. (1973) *Biochim. Biophys. Acta 302*, 443−456.
8. Tietz, A., and Ochoa, S. (1958) *Arch. Biochem. Biophys. 78*, 477−493.
9. Lodato, D. T., and Reed, G. H. (1987) *Biochemistry 26*, 2243−2250.
10. Reed, G. H., and Morgan, S. D. (1974) *Biochemistry 13*, 3537−3541.
11. Buchbinder, J. L., and Reed, G. H. (1990) *Biochemistry 29*, 1799−1806.
12. Buchbinder, J. L., Baraniak, J., Frey, P. A., and Reed, G. H. (1993) *Biochemistry 32*, 14111−14116.
13. Kofron, J. L., and Reed, G. H. (1990) *Arch. Biochem. Biophys. 280*, 40−44.
14. Muirhead, H., Clayden, D. A., Barford, D., Lorimer, C. G., Fothergill-Gilmore, L. A., and Schmitt, W. (1986) *EMBO J. 5*, 475−481.
15. Larsen, T. M., Laughlin, L. T., Holden, H. M., Rayment, I., and Reed, G. H. (1994) *Biochemistry 33*, 6301−6309.
16. Larsen, T. M., Benning, M. M., Wesenberg, G. E., Rayment, I., and Reed, G. H. (1997) *Arch. Biochem. Biophys. 345*, 199−206.
17. Walker, J. E., Saraste, M., Runswick, J. M., and Gay, N. J. (1982) *EMBO J. 1*, 945−951.
18. Milner-White, E. J., Coggins, J. R., and Anton, I. A. (1991) *J. Mol. Biol. 221*, 751−754.
19. Teng, T.-Y. (1994) *J. Appl. Crystallogr. 23*, 387−391.
20. Rodgers, D. W. (1997) *Methods Enzymol. 276*, 183−203.
21. Navaza, J. (1987) *Acta Crystallogr. A43*, 645−653.
22. Navaza, J. (1990) *Acta Crystallogr. A46*, 619−620.
23. Tronrud, D. E., Ten Eyck, L. F., and Matthews, B. W. (1987) *Acta Crystallogr. A43*, 489−501.
24. Jones, T. A. (1985) *Methods Enzymol. 115*, 157−171.
25. Jones, T. A., Zou, J.-Y., Cowan, S. W., and Kjeldguard, M. (1991) *Acta Crystallogr. A47*, 110−119.
26. Lu, A., Shorter, A. L., and Dunaway-Mariano, D. (1993) *Biochemistry 32*, 2378−2385.
27. Jaffe, E. K. (1979) Ph.D. Dissertation, University of Pennsylvania, Philadelphia, PA.
28. Kayne, F. J. (1973) *Enzymes* (*3rd Ed.*) *8*, 353−382.
29. Bezares, G., Eyzaguirre, J., Hinrichs, M. V., Heinrikson, R. L., Reardon, I., Kemp, R. G., Latshaw, S. P., and Bazaes, S. (1987) *Arch. Biochem. Biophys. 253*, 133−137.
30. Kobayashi, N., and Go, N. (1997) *Nat. Struct. Biol. 4*, 6−7.
31. Tari, L. W., Matte, A., Pugazhenthi, U., Goldie, H., & Belbaere, L. T. J. (1996) *Nat. Struct. Biol. 3*, 355−363.
32. Tari, L. W., Matte, A., Goldie, H., & Delbaere, L. T. J. (1997) *Nat. Struct. Biol. 4*, 990−994.
33. Kayne, F. J. (1971) *Arch. Biochem. Biophys. 143*, 232−239.
34. Blättler, W. A., and Knowles, J. R. (1979) *Biochemistry 18*, 3927−3933.
35. Knowles, J. R. (1980) *Annu. Rev. Biochem. 49*, 877−919.
36. Reed, G. H., and Cohn, M. (1973) *J. Biol. Chem. 248*, 6436−6442.
37. Robinson, J. L., and Rose, I. A. (1972) *J. Biol. Chem. 247*, 1096−1105.
38. Gupta, R. K., Oesterling, R. M., and Mildvan, A. S. (1976) *Biochemistry 15*, 2881−2887.
39. Gupta, R. K., and Mildvan, A. S. (1977) *J. Biol. Chem. 252*, 5967−5976.
40. Cornelius, R. D., Hart, P. A., and Cleland, W. W. (1977) *Inorg. Chem. 16*, 2799−2805.
41. Block, H., and Gold, V. (1959) *J. Chem. Soc.*, 966−975.
42. Rose, I. A., and Kuo, D. J. (1989) *Biochemistry 28*, 9579−9585.
43. Rose, I. A., Kuo, D. J., and Warms, J. V. B. (1991) *Biochemistry 30*, 722−726.
44. Bai, Y., Milne, J. S., Mayne, L., and Englander, S. W. (1993) *Proteins: Struct., Funct., Genet. 17*, 75−86.
45. Laskowski, R. A., MacArthur, M. W., Moss, S. S., and Thornton, J. M. (1993) *J. Appl. Crystallogr. 26*, 283−291.
46. Kraulis, P. J. (1991) *J. Appl. Crystallogr. 24*, 946−950.

BI980243S